Carbonell Alcaina, C.; Corbatón Báguena, MJ.; Alvarez Blanco, S.; Bes-Piá, M.; Mendoza Roca, JA.; Pastor Alcañiz, L. (2016). Determination of fouling mechanisms in polymeric ultrafiltration membranes using residual brines from table olive storage wastewaters as feed. Journal of Food Engineering. 187:14-23. doi:10.1016/j.jfoodeng.2016.04.016

Determination of fouling mechanisms in polymeric ultrafiltration membranes using residual brines from table olive storage wastewaters as feed

Carlos Carbonell-Alcaina[1], María-José Corbatón-Báguena[1], Silvia Álvarez-Blanco[1,2], M. Amparo Bes-Piá[1,2], José Antonio Mendoza-Roca[1,2], Laura Pastor-Alcañiz[3]

[1]*Research Institute for Industrial, Radiophysical and Environmental Safety (ISIRYM), Universitat Politècnica de València, C/Camino de Vera s/n, 46022 Valencia, Spain.*

[2]*Department of Chemical and Nuclear Engineering, Universitat Politècnica de València, C/Camino de Vera s/n, 46022 Valencia, Spain*

[3]*Depuración de Aguas del Mediterráneo (DAM), Avda. Benjamin Franklin, 21, Parque Tecnológico, 46980 Paterna (Valencia)*

*Corresponding author: Carlos Carbonell-Alcaina

E-mail addresses: carcaral@upvnet.upv.es

Phone: +34 963879630

Fax: +34 96 3877639

Abstract

In this work, the fouling mechanisms that dominate the ultrafiltration of residual brines from table olive packing plant wastewaters were investigated. For that purpose, Hermia's models adapted to crossflow filtration, resistance-in-series model and a model combining intermediate blocking and cake formation mechanisms were fitted to the

experimental data. Tests were performed with a 5kDa polyethersulfone membrane at transmembrane pressures between 1-3 bar and crossflow velocities between 2.2-3.7 $m \cdot s^{-1}$. Results demonstrated that the resistance-in-series model was the most accurate to predict permeate flux evolution with time. The predominant fouling mechanism was cake formation followed by intermediate blocking/adsorption. The fouling resistances that were determined by means of the resistance in series model were tested using a well-established mathematical model proposed by Mondal and De that also combines both fouling phenomena (intermediate pore blocking and cake formation). Results demonstrated that the predicted resistances are consistent with those determined by Mondal and De's model.

Keywords: Ultrafiltration; polyethersulfone membranes; table olive packing plant wastewaters; mathematical models; fouling mechanisms.

1. Introduction

Spain is the main producer of table olives with 573 500 $t \cdot year^{-1}$, which is around 22.1 % of the total world production (International Olive Oil Council 2014). During the production process, large amounts of water are used, generating high volumes of wastewater. Three types of wastewater are obtained: debittering, washing and fermentation brines (Benitez et al. 2003). Fermentation brine wastewater is characterized by an acidic pH (around 4), a high conductivity (80-115 $mS \cdot cm^{-1}$), a high concentration of total suspended solids (0.2-2 $g \cdot L^{-1}$), dissolved chemical oxygen demand (COD: 10-35 g $O_2 \cdot L^{-1}$) and phenolic compounds (4.0-6.0 g of tannic $acid \cdot L^{-1}$) (Garrido Fernández et al. 1997). Ultrafiltration (UF) is one of the most used techniques

in industry to: concentrate, separate or purify macromolecules, colloids and suspended particles from liquid streams (Wang and Song, 1999; Barredo-Damas et al. 2012). In this work, UF is considered to remove suspended particles and macromolecules from residual brines from table olive production plants. A subsequent nanofiltration (NF) step could be performed to recover the phenolic compounds.

Currently there are many studies focused on membrane treatment of wastewaters from olive oil production, such as, olive mill wastewater (OMW) residue from a three-phase production method and alperujo residue from a two-phase production method. These residues have a high chemical oxygen demand and a high phenolic compound concentration, but unlike fermentation brine, its conductivity is much lower (between 4.00-13.98 $mS \cdot cm^{-1}$ for OMW and 0.88-4.76 $mS \cdot cm^{-1}$ for alperujo) (Paredes et al. 1999; Alburquerque et al. 2004). Nanofiltration (NF) processes have been considered by most of the authors to recover and concentrate high added value compounds from olive oil production wastewaters. In order to improve the performance of the NF process, a pre-treatment with UF has also been proposed (Galanakis et al. 2010; Paraskeva et al. 2007). However, the number of studies on the treatment of fermentation brine wastewater by membrane technology is very limited. Nowadays, the technologies that have shown more favorable results for recovering desirable compounds from the brines have been membrane processes. This can be combined with adsorption processes using active carbon or ion exchange resins (Bódalo et al. 2008). The rejection of total suspended solids, dissolved COD and phenolic compounds in UF process treating olive mill wastewater (OMW) and table olive wastewaters was investigated by El-Abbassi (El-Abbassi et al. 2014).

Membrane fouling is one of the major problems of UF processes, reducing the permeate flux and decreasing its economic and technological viability (Cheryan and Alvarez, 1995). During an UF process where fouling occurs, the initial permeate flux shows a sharp decline which is followed by a long and gradual flux decline over time (Field et al. 1995). Therefore, the study of the evolution of permeate flux over time during UF is an important factor to be considered when selecting the optimum operating conditions (Vincent-Vela et al. 2010). In order to predict the UF membrane fouling and its performance, mathematical models have been developed by several authors. In literature, empirical and theoretical models that describe the permeate flux decline, with time in UF, can be found. Empirical models provide high precision, but they cannot satisfactorily explain the fouling mechanisms involved in membrane filtration. Theoretical models can help to better understand the phenomenon of fouling, but if experimental data is not used to estimate some of the parameters their predictions are not very precise. Thus, semi-empirical models whose parameters have a physical meaning are usually preferred to explain the fouling phenomena that takes place in membrane processes and to achieve an accurate prediction of permeate flux decline (Vincent Vela et al. 2009; Mah et al. 2012). Depending on the fouling mechanism, four situations may be described: (a) if the solute particle size is higher than the membrane pore; particles are deposited on the surface of the membrane blocking the entrances of the pores completely; (b) if solute particle and membrane pores size are similar, some membrane pores can be partially blocked; (c) if solute particle size is smaller than membrane pores, inside pores of membrane can be blocked and irreversible fouling may appear; (d) sometimes the fouling layer deposited on the membrane surface may form a cake layer (Ruby Figueroa et al. 2011; Corbatón-Báguena et al. 2013).

Among the different theoretical models available in the literature to determine fouling mechanisms, one of the most widely used is the one developed by Ho and Zydney (Ho and Zydney, 2000). The general equation of this model accounts for the combination of pore blockage and cake formation without time division of the permeate flux curve. The authors fitted the model to the BSA microfiltration experimental data. Based on the Ho and Zydney's model, recent works have used their mathematical assumptions to fit the experimental data of different UF processes and also, modify the original model (Muthukumaran et al., 2005; Peng and Tremblay, 2008; Karasu et al., 2010; Corbatón-Báguena et al., 2013; Liu et al., 2014; Tien et al., 2014; Astaraee et al., 2015). For instance, Astaree et al. studied membrane fouling mechanisms caused by BSA, dextran and humic acid solutions by fitting the model proposed by Ho and Zydney and modifying it to consider the hydrophilic nature of the membranes used and the pre-filtration effect of the foulant deposit layer. With these two new factors, they demonstrated that better agreements were obtained in comparison to the original mathematical model (Astaree et al., 2015). On the other hand, Tien et al. used the experimental data presented by Ho and Zydney to validate their new rational model, which was based on the deep bed filtration theories and the equations for particle retention within membrane media. Their model was able to predict the experimental data provided by Ho and Zydney and its general equation was simpler than the original one (Tien et al., 2014).

In the same way as Ho and Zydney, some other authors combined two different fouling mechanisms providing a model with strong theoretical background. For instance, Mondal and De published two different articles which describe in detail a generalized model for steady state continuous filtration (Mondal and De, 2009; Mondal and De,

2010). The proposed model resulted from the combination of two different fouling mechanisms: on their first article, Mondal and De took into account the resistance due to complete pore blocking and that related to the formation of a cake on the membrane surface (Mondal and De, 2009); while the second article combined the resistances due to intermediate pore blocking and cake formation mechanisms (Mondal and De, 2010). In addition, Bolton et al. developed five new models based on the four classical fouling mechanisms (standard blocking, complete and intermediate blocking and cake formation mechanisms) and the Darcy's law for both constant pressure and constant flow operation modes (G. Bolton et al., 2006). Their theoretical hypotheses resulted in general equations with two fitting parameters that were much simpler than those taken as references by the authors. Their results also demonstrated that the new models predicted with good accuracy the experimental data. Using the equations developed by Bolton et al., other authors, such as Rezaei et al., fitted those general equations for the combined models to the experimental data obtained during whey crossflow microfiltration (Rezaei et al., 2011). They also compared the fitting accuracies of the combined models with the classical ones that account only for one fouling mechanism at a time. Their results demonstrated that the combined models were able to better predict the permeate flux decline at low time scales, but classical models provided higher accuracies at those experimental conditions where cake resistance was the predominant fouling mechanism.

Although there are several mathematical models available in the literature to determine fouling mechanisms, Hermia's models and their adaptations to crossflow filtration as well as resistance-in-series models are the most accepted. These have also been used to predict permeate flux decline, with time, by other authors (Carrère et al. 2001; Turano et

al. 2002; Vincent Vela et al. 2009). Vincent Vela *et al.* (2009) fitted the Hermia's models adapted to crossflow to the experimental data of permeate flux versus time obtained during the UF of polyethylene glycol solutions. They demonstrated that at high transmembrane pressures and low crossflow velocities, the intermediate blocking was the predominant fouling mechanism. Corbatón-Báguena *et al.* (2015a) fitted different models to the experimental data obtained during the UF of whey model solutions. They reported that the combination of complete blocking and cake formation mechanisms resulted in more accurate predictions of the permeate flux decline. Carrère *et al.* (2001) proposed a resistance-in-series model that considered the membrane resistance, the cake resistance and the adsorption and concentration polarization resistance. This was done to estimate permeate flux decline in the crossflow microfiltration of lactic acid fermentation broths. They reported that the adsorption and concentration polarization resistances dominated the filtration process. Turano *et al.* (2002) also interpreted the experimental data of permeate flux variation with the time obtained during the UF of olive mill wastewaters by using a resistance-in-series model. They indicated that higher values of turbulence and thus higher crossflow velocities resulted in lower values of specific cake resistance.

In this work, the effect of transmembrane pressure (TMP) and crossflow velocity (CFV) on flux decline when UF was used to treat residual brine from a table olives packing plant (TOPP) was investigated. The samples were previously filtered through a 60 μm cartridge filter. In order to understand the predominant fouling mechanisms affecting permeate flux decline when UF membranes were fouled with the residual brine, several mathematical models were taken into account: Hermia's models adapted to crossflow filtration, a resistance-in-series model and a model that combines the complete blocking and cake formation fouling mechanisms developed by Hermia. It is important to

highlight the practical relevance of this type of empirical models based on exponential equations, since recent works were published at this regard. For instance, Lin et al. used an exponential model with four fitting parameters to predict the entire permeate flux curve obtained in the ultrafiltration of protein aqueous solutions (Lin et al., 2008). They divided the decrease in permeate flux according to two fouling phenomena: intermediate blocking for the first minutes of operation and cake formation fouling for the rest of the ultrafiltration curve. Yee et al. studied the crossflow ultrafiltration of whey by fitting an exponential equation to the experimental data obtained in the fouling experiments (Yee et al., 2009). The empirical model was compared to Ho and Zydney's one, and fitting results demonstrated that the theoretical Ho and Zydney's model did not provide high accuracies at great time scales. However, model fittings using the exponential pattern were in a good agreement with the experimental data. Corbatón-Báguena et al. used empirical models with theoretical background to fit the experimental data obtained during the ultrafiltration of enzymatic solutions (Corbatón-Báguena et al., 2015b). These models were based on exponential decay patterns whose main parameters have physical meaning (for instance, ratio among original membrane characteristics and those achieved after fouling and resistances due to complete blocking and cake formation). In the literature, most of the mathematical models were tested with model solutions instead of real solutions. Moreover, the fouling mechanism that causes flux reduction when table olive residual brine is ultrafiltered has not been investigated so far. In addition, Astudillo-Castro explained the fundamentals of the exponential equations proposed in this work, which are based on the direct relationship between the maximum resistance value (achieved at the steady state) and that obtained at a certain time (Astudillo-Castro, 2015). These authors applied the abovementioned mathematical equations to describe the limiting permeate flux as a function of

transmembrane pressure. Another novelty of this work corresponds to the validation of the fitted parameters obtained using a well-established, theoretical model available in the literature (resistance in series model developed by Mondal and De, 2010).

2. Ultrafiltration modelling

2.1. Hermia's models adapted to crossflow filtration

Based on the classical Hermia's models for constant pressure dead-end filtration (Hermia 1982), several authors (Field et al. 1995; de Barros et al. 2003; Vincent Vela et al. 2009) included the steady-state flux related to the back-transport mass transfer to adapt the classical models to a crossflow configuration. Eq. 1 shows the general model equation for the adapted Hermia's models:

$$-\frac{dJ}{dt} = K\left(J - J_{ss}\right)J^{2-n} \qquad (1)$$

where J is the permeate flux, J_{ss} is the steady-state permeate flux, K is the model constant and n is the model parameter related to the four different fouling mechanisms. If the value of n is zero, a cake layer is formed on the membrane surface due to the accumulation of solute molecules that are larger than membrane pores. When $n = 1$, the fouling mechanism corresponds to the intermediate blocking model, which considers that foulant molecules cannot penetrate inside the porous structure and are deposited on previously settled molecules. The complete blocking model ($n = 2$), occurs when a solute molecule completely seals a pore entrance without penetrating inside the membrane pores and solute molecules form a monomolecular layer on the membrane

surface. Finally, solute molecules that have a smaller size than the membrane pores can pass through the porous structure and block the inner pore walls. This corresponds to the standard blocking model (n = 1.5).

2.2. Combined model (intermediate pore blocking and cake formation)

According to the literature (Field et al. 1995; Ho and Zydney, 2000), the typical evolution of permeate flux during the UF time can be divided in two stages: a great decline in permeate flux during the first minutes of operation because of a pore blocking phenomenon and a gradually slow flux decline caused by the accumulation of foulant molecules on the membrane surface and the formation of a cake layer on it. Along with this evolution, de la Casa *et al.* (2008) developed a combined model taking into account the classical dead-end Hermia's equations for the complete blocking and cake formation model. In this work, a similar combination of the intermediate pore blocking and cake formation models described by Hermia was adapted to crossflow operating mode (Eq. 2):

$$J_{\text{combined model}} = \alpha \cdot J_{\text{intermediate blocking model}} + (1-\alpha) \cdot J_{\text{cake layer formation model}} \qquad (2)$$

where α is the fraction of blocked membrane pores. In addition, Eq. 2 includes two different model constants (K_i for the intermediate blocking model and K_{cf} for the cake layer formation model) as they are the constants that correspond to Hermia's equations adapted to crossflow operation for the intermediate pore blocking and the cake formation models, respectively. The physical meaning of these two parameters is the following: K_i represents the membrane surface blocked per unit of total permeate

volume and unit of initial membrane surface porosity, while K_{cf} is the ratio between the characteristics of the cake layer on the membrane surface and those of the original, unfouled membrane (Vincent-Vela *et al.*, 2009).

2.3. Resistance-in-series model

The resistance-in-series model is based on the Darcy's law, which relates the permeate flux (J) with the transmembrane pressure (ΔP), the feed solution viscosity (μ) and the total hydraulic resistance (R_t) (Eq. 3).

$$J = K \cdot \Delta P = \frac{\Delta P}{\mu \cdot R_t} \tag{3}$$

This model describes the total hydraulic resistance during the filtration process as the sum of several resistances: the original membrane resistance (R_m), the adsorption and concentration polarization resistance (R_a) and the cake layer resistance (R_{cf}) (Eq. 4) (Choi et al. 2000; Carrère et al. 2001; Turano et al. 2002):

$$R_t = R_m + R_a + R_{cf} \tag{4}$$

According to Carrère et al., the experimental variation of R_t, R_a and R_{cf} follows an exponential trend (Carrère et al., 2001; Carrère et al., 2002). In addition, both adsorption and concentration polarization phenomena are simultaneously determined in crossflow filtration experiments. Thus, R_a can be expressed as an exponential function of the steady-state resistance (R'_a), the rate of molecules deposition on the membrane surface

(*b*) and the filtration time (*t*), according to Eq. 5. Based on Eq. 5, in this work a general equation that account for R_{cf} as a function of time was newly proposed and represented in Eq. 6, where R'_{cf} is the steady-state cake resistance and *c* is the rate of cake growth:

$$R_a = R'_a\left(1-\exp\left(-b\cdot t\right)\right) \tag{5}$$

$$R_{cf} = R'_{cf}\left(1-exp\left(-c\cdot t\right)\right) \tag{6}$$

Substituting Eq. 5 and Eq. 6 in Eq. 4 and considering the Darcy's law (Eq. 3), the general equation for the resistance-in-series model can be obtained (Eq. 7):

$$J = \frac{\Delta P}{\mu\cdot\left(R_m + R'_a\left(1-exp\left(-b\cdot t\right)\right) + R'_{cf}\left(1-exp\left(-c\cdot t\right)\right)\right)} \tag{7}$$

2.4. Validation of resistance-in-series model

The constants obtained in this work for the resistance-in-series model were validated using a model developed by Mondal and De, 2010. This model is also based on the resistance in series mechanism and combines the resistances of two classical fouling mechanisms (intermediate pore blocking and cake formation). According to this model, at low time scales (up to a certain time point, t_1), membrane fouling resistance is due to the intermediate pore blocking phenomenon and as a result, permeate flux sharply declines with time (Eq. 8). Therefore, permeate flux variation with time can be described as:

$$J = \frac{\Delta P}{\mu \cdot \left(R_m + R_{IPB} \right)} \tag{8}$$

where R_{IPB} is the intermediate pore blocking resistance. This resistance can be expressed as a function of time by means of the intermediate pore blocking constant (K_{IPB}), according to Eq. 9. Therefore, the general model equation up to t_1 is Eq. 10.

$$R_{IPB} = \frac{\Delta P}{\mu} \cdot K_{IPB} \cdot t \tag{9}$$

$$J = \frac{\Delta P}{\mu \cdot \left(R_m + \frac{\Delta P}{\mu} \cdot K_{IPB} \cdot t \right)} \tag{10}$$

For time scales from t_1 to the end of the filtration process, the formation of a cake on the membrane surface becomes the predominant fouling mechanism and therefore, the general model equation considers the effect of cake formation from t_1 to the end of the filtration process as well as the effect of intermediate pore blocking at t_1. Then permeate flux decline with time is described by Eq. 11:

$$J = \frac{\Delta P}{\mu \cdot \left(R_m + R_{IPB}\left(t_1\right) + R_{cf}\left(t - t_1\right) \right)} \tag{11}$$

Therefore, in order to validate the constants obtained for the resistance-in-series model, Eq. 10 was firstly fitted to the experimental data up to the selected t_1 values for each experimental condition tested. Once the values of K_{IPB} were obtained, the resistance

R_{IPB} was calculated using Eq. 9 and the predicted values of permeate flux for low time scales were determined. After that, using the value of R_{IPB} at time t_1 and substituting the values of R_{cf} from the resistance-in-series model (described in section 2.3) in Eq. 11, the predicted values of permeate flux for time scales greater than t_1 were determined. Finally, the permeate flux predicted values were compared to the experimental data and to the resistance in series method data. The goodness of the fits (in terms of R^2 and *SD*) was determined.

3. Materials and methods

3.1. Feed samples

This work was performed using different real solutions from residual table olive brine, supplied by a TOPP. Due to the high suspended solids content, a filtration step with a polyester cartridge filter of 60 μm pore was carried out. Four different samples were provided by the TOPP. The average characteristics of the filtered samples are shown in Table 1. The samples were stored at 5 °C.

Table 1. Characteristics of feed filtered with a 60 μm polyester cartridge filter (mean values for all the feed samples).

Parameter	Mean value	Standard Deviation
pH	4.0	± 0.2
Conductivity (mS/cm)	85.3	± 12.1
Turbidity (NTU)	262.8	± 92.8
TSS (mg/L)	411.7	± 80.0
Dissolved COD (mg/L)	16547.7	± 3902.0
Phenolic compounds (mg/L Tyrosol eq)	1100.9	± 325.7

3.2. Analytical methods

Feed and permeate samples were characterized. The pH and the conductivity were measured with a pH-Meter GLP 21+ and EC-Meter GLP 31+ (Crison, Spain). Total suspended solids (TSS) were determined according UNE 77034 by means of glass microfibre filters with 1.2 μm pore size, using samples of 25 mL and differing weights before and after drying the microfibre filters at 105ºC, for 2 hours. Turbidity was measured considering the UNE-EN ISO 7027 standard method with a turbidimeter (D-112, DINKO, Spain). Dissolved COD was determined with Hach Lange kits, LCK014 (LCK, Germany), dissolving the samples 10-12 times in order to remove the interferences caused by the high chloride concentration.

3.3. Equipments and procedures

3.3.1. Ultrafiltration

The feed samples for the UF process were residual olive brine from a TOPP. This had been previously filtered using a 60 μm polyester mesh cartridge filter (CA-0202-00, model GT). The automated UF laboratory plant regulated transmembrane pressure (TMP), cross flow velocity and temperature. A Rayflow membrane module from Orelis (France) was utilized, configured to work with only one membrane in cross-flow mode. A Microdyn Nadir (Germany) polyethersulfone (PES) membrane with a MWCO of 5 kDa (Nadir UP005) was tested. The total active surface of the membrane was 0.0125 m^2. The R_m value for the UP005 membrane used in the experiments was $8.9216 \cdot 10^{12} \pm 0.8057 \cdot 10^{12}$ m^{-1}, obtained from the observed linear relationship between pure water permeate flux and TMP ($R^2 = 0.9965 \pm 0.0030$). Darcy´s law (Eq. 3) was used for the

calculation. This value was considered as a constant to fit the resistance-in-series model to the experimental data.

Fouling and cleaning tests were carried out with varying TMP and CFV, set at 1-3 bar and 2.2-3.7 $m \cdot s^{-1}$ respectively, for 2.5 hours. During this time temperature was kept at a constant 25ºC. After this period, steady state was achieved, allowing permeate and retentate to be recycled back to the feed tank. Permeate flux was monitored with a precision balance from Kern (Germany) and the collected data was recorded with a data acquisition system. After each run, it was checked that if was restored to the initial permeability. A permeability recovery higher than 95% was required before further testing could be carried out. Membrane cleaning was performed by rinsing with osmotic water at CFV of 2.2 $m \cdot s^{-1}$ and TMP of 0.6 bar during 9 minutes. If the initial permeability was not restored membrane was cleaned with chemicals using a concentrated basic solution of NaOH (pH 11) (Panreac, Spain) and acid solution in water of citric acid (1% w/v) (Panreac, Spain) at CFV of 2.2 $m \cdot s^{-1}$ and TMP of 0.6 bar during 5 minutes, respectively. After each chemical cleaning, the system was rinsed with osmotic water at the same operating conditions for other 9 minutes.

3.4. Model fitting

The model was fitted to the experimental data using MathCad® 15 (PTC Needham, EE.UU). This was carried out by means of the MathCad® Genfit algorithm, which uses an optimized version of the Levenberg-Marquadt method, minimizing the difference between the predicted and experimental results. The quality of the fitting for each

operating condition tested was evaluated in terms of the regression coefficient (R^2) and the standard deviation (SD).

4. Results and discussion

Figs. 1 to 3 show the variation of permeate flux with time for the combinations of TMP and CFV tested.

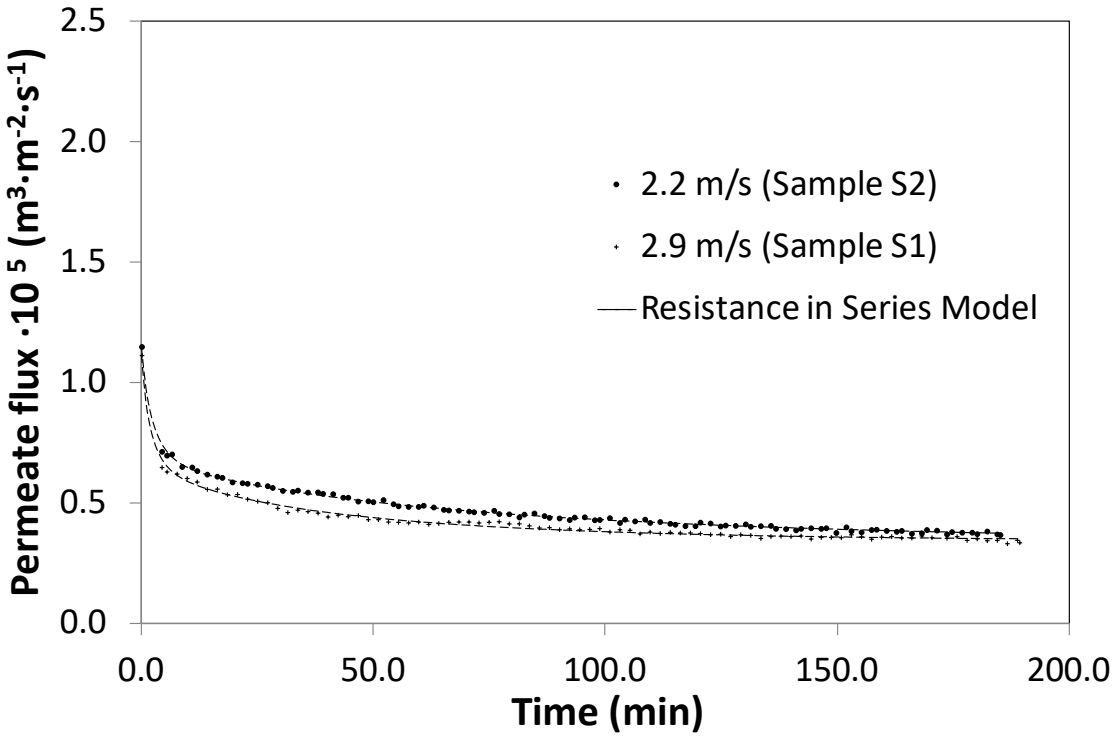

Fig. 1 Evolution of permeate flux with time during the UF experiments at TMP of 1 bar and model fitting to the experimental data.

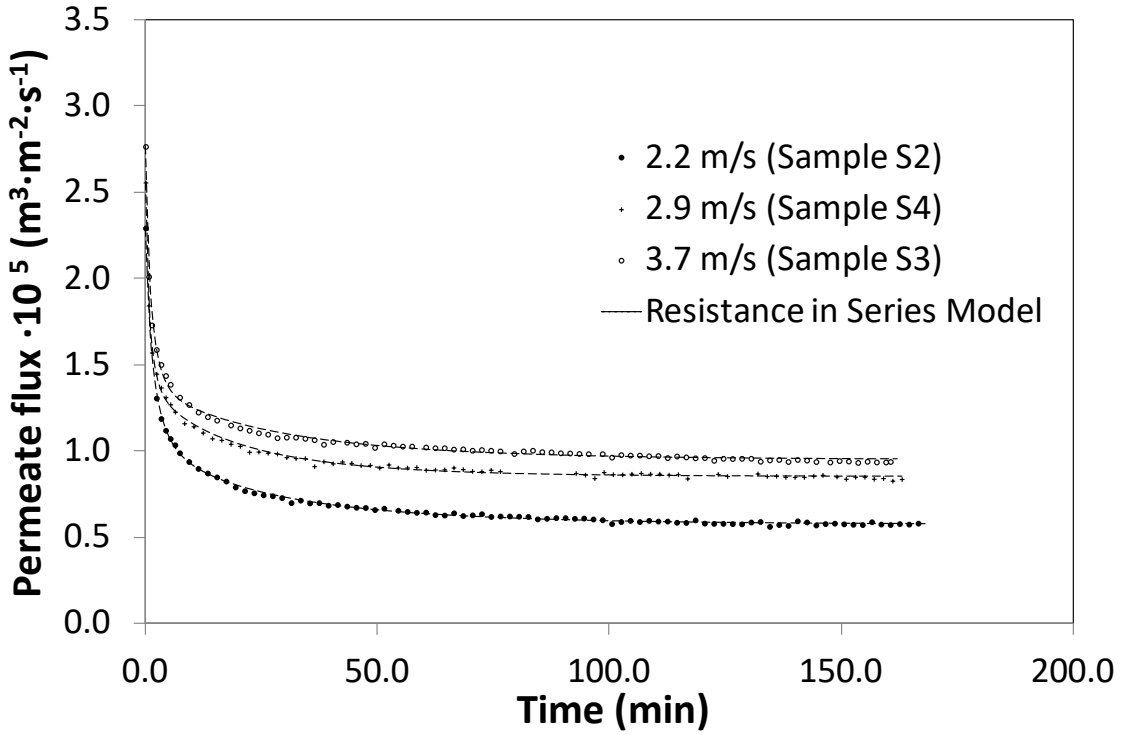

Fig. 2 Evolution of permeate flux with time during the UF experiments at TMP of 2 bar and model fitting to the experimental data.

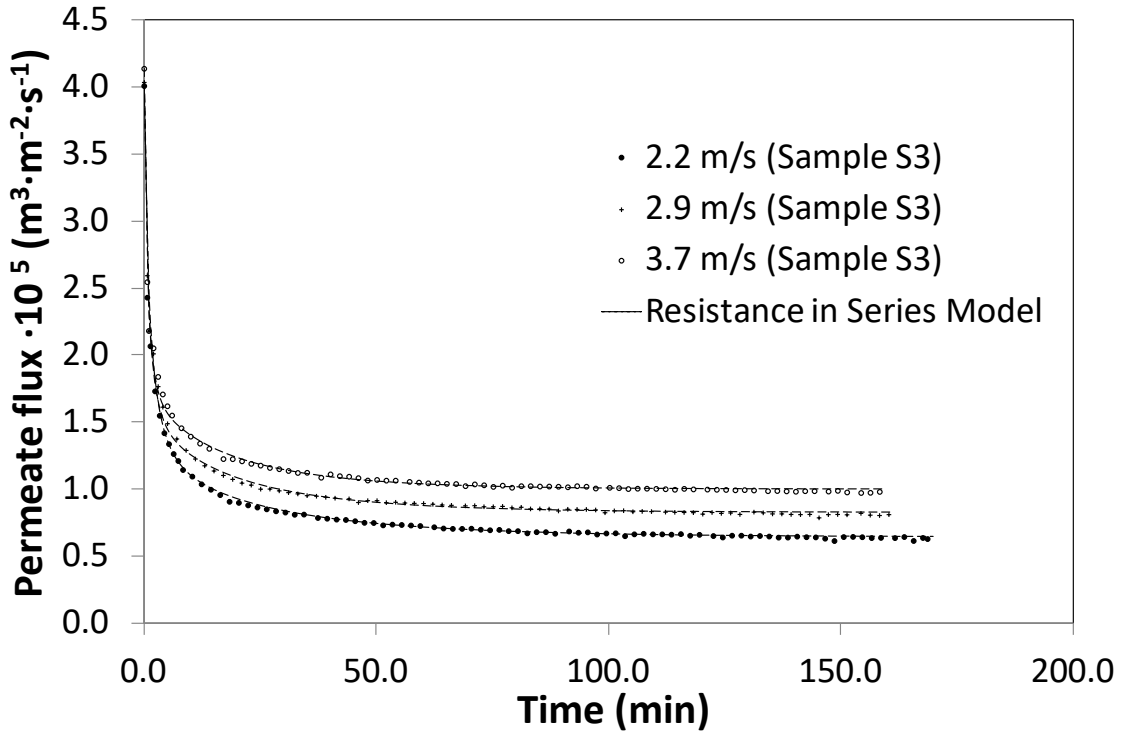

Fig. 3 Evolution of permeate flux with time during the UF experiments at TMP of 3 bar and model fitting to the experiment data.

As it can be observed, the values of steady state permeate flux were low for all the operating conditions tested because of fouling. At a TMP of 1 bar, the variation of CFV within the range considered in this work did not produce significant variations in permeate flux. However, at 2 and 3 bar flux variation with TMP at certain CFV was lower than flux variation with CFV at certain TMP. Therefore, these tested pressures were in the range where flux reaches the critical flux, as it can be observed from Fig. 4. In this figure the stationary permeate flux is plotted against TMP for the different CFV tested. It is observed that the stationary permeate fluxes are far from the osmotic water line. The stationary permeate flux increased with TMP up to a point at which permeate flux remains constant or decreases with TMP. In this region, if pressure increases, an increase in particle concentration on the membrane boundary layer takes place (Miller et al. 2014). The presence of a high concentration of solutes in table olive residual brine has a great effect on their concentration in the mass transfer boundary layer as well as on the membrane surface, affecting the development of the gel layer. Therefore, the effect of TMP and CFV on concentration polarization is significant (Mondal et al. 2011). Thus, as it can be observed in Figs. 1-3, permeate flux decline decreases with CFV and increases with TMP.

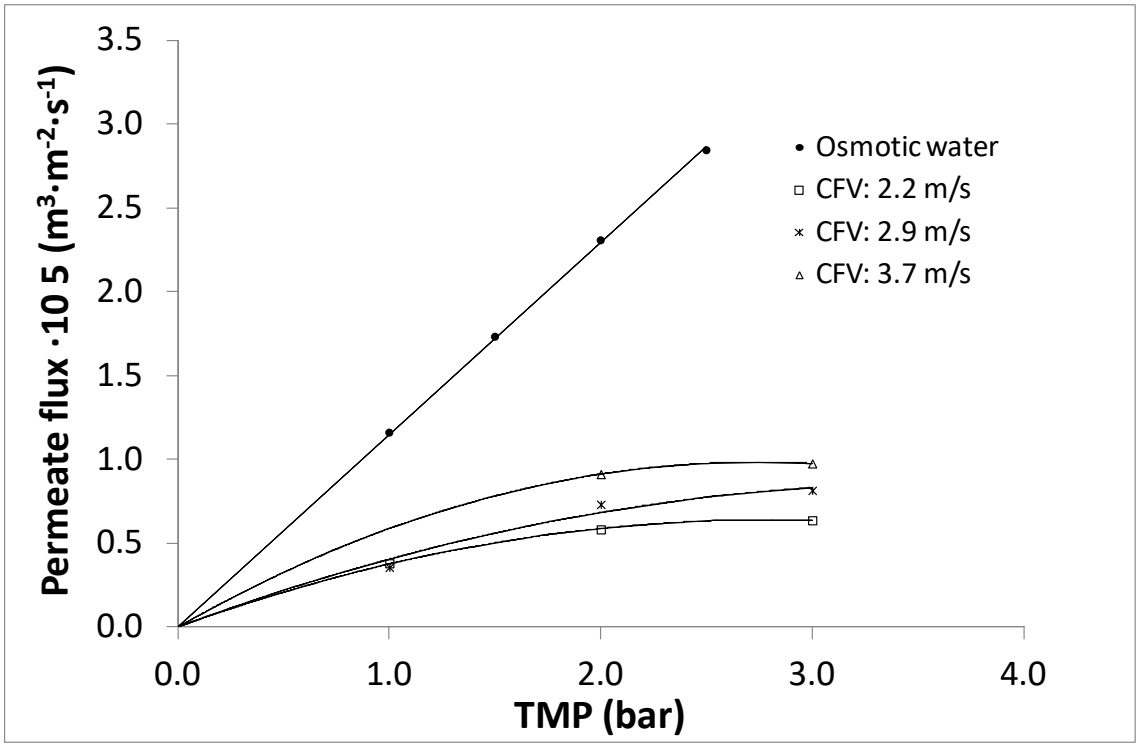

Fig. 4 Steady state permeate flux versus transmembrane pressure (TMP) for the different crossflow velocities (CFV) tested.

4.1. Modelling results

The evolution of permeate flux with time during the UF experiments for each transmembrane pressure, crossflow velocity and feed solution tested is shown in Figs. 1 to 3. As transmembrane pressure increased, flux decline during the first minutes of operation was more rapid, as it was expected (Ho and Zydney, 2000). This behaviour corresponded to the existence of pore blocking phenomena, which are mostly responsible for membrane fouling at low time scales. In addition, the higher the crossflow velocity was, the higher the steady-state permeate flux was. According to other authors (Lin et al. 2004), the shear stress and turbulence produced by an increase in crossflow velocity may prevent membrane surface from severe fouling. Therefore, the permeate flux achieved at the end of the UF run increased as CFV increased.

The percentage of flux decline reached at the end of the UF experiments for each feed solution and operating conditions tested is shown in Table 2. As it can be observed, permeate flux decline significantly increased as the transmembrane pressure applied increased from 1 to 3 bar. For instance, for the sample S2, flux decline increased from 69.02 to 74.91 % when the transmembrane pressure increased from 1 to 2 bar at a given crossflow velocity (2.2 $m \cdot s^{-1}$). In addition, for the sample S3, at 3.7 $m \cdot s^{-1}$, permeate flux decline increased from 65.77 to 76.40 % from 2 to 3 bar. The initial permeate flux decline rate increases with transmembrane pressure due to the higher initial flux generated by TMP, which allows the passage of more water through the membrane, before the concentration polarization phenomenon was entirely developed (Chen and Kim, 2006). Moreover, as TMP increases there is a greater transport of solute molecules towards the membrane surface due to the increase in the driven force. Thus, a greater decrease in permeate flux was observed at high transmembrane pressures.

Table 2. Percentage of flux decline at the end of the UF experiments.

TMP[a] (bar)	CFV[b] ($m \cdot s^{-1}$)	Sample	Feed turbidity (NTU)	Flux decline (%)
1	2.2	S2	314.3	69.02
	2.9	S1	367.5	68.97
2	2.2	S2	314.3	74.91
	2.9	S2	314.3	72.39
	2.9	S4	183.4	67.26
	3.7	S3	185.9	65.77
	3.7	S4	183.4	64.65
3	2.2	S3	185.9	84.22
	2.2	S1	367.5	86.53
	2.9	S3	185.9	79.98
	3.7	S3	185.9	76.40

[a]TMP: transmembrane pressure; [b]CFV: crossflow velocity.

On the other hand, the trend observed as the crossflow velocity increased was the opposite as that reported for the transmembrane pressure, as expected, since permeate

flux decline decreased with crossflow velocity for a fixed value of transmembrane pressure. Crossflow velocity has a favourable influence on membrane filtration performance: the shear stress caused at high crossflow velocities may reduce concentration polarization and solute precipitation, preventing the membrane from a severe fouling (Lin et al. 2004). Therefore, the greatest the crossflow velocity was for a given transmembrane pressure, the lowest the permeate flux decline was.

The effect of turbidity on flux decline is also observed in Table 2. This table shows that, for the same operating conditions, flux decline increased when turbidity increased (for example when samples S2 and S4 are treated at 2 bar and 2.9 $m \cdot s^{-1}$). It ca be also observed that flux decline was greater for sample S1 at 1 bar and 2.9 $m \cdot s^{-1}$ than that for sample S4 at 2 bar and 2.9 $m \cdot s^{-1}$. This is due to the effect of turbidity, which caused higher flux reduction even at lower transmembrane pressures. Sample S4 was much more turbid than sample S1. This effect was not observed however when flux decline for sample S1 at 1 bar and 2.9 $m \cdot s^{-1}$ is compared to flux decline for sample S2 at 2 bar and 2.9 $m \cdot s^{-1}$, because the difference between their turbidity was much lower.

Table 3 shows the fitting accuracy results for all the models tested in terms of the regression coefficient (R^2) and standard deviation (SD). The values of R^2 and SD for the model with the highest fitting accuracy are highlighted in bold in the table. It is important to highlight that Hermia's standard blocking model adapted to crossflow did not fit to the experimental data. This model considers that solute molecules are smaller than membrane pore size and thus they can penetrate inside the membrane porous structure. Therefore, it can be concluded that internal pore blocking is not significant. As it can be observed, the predictions of the resistance-in-series and combined models

were the most accurate for all the transmembrane pressures, crossflow velocities and feed solutions tested. At 2 and 3 bar, the accuracy of both models was similar. However, at 1 bar, the accuracy of the combined model was worse than the accuracy of the resistance-in-series model. Values of R^2 and SD for the resistance-in-series model ranged from 0.953 to 0.996 and 0.040 to 0.016, respectively. Figs. 1 to 3 show the fitting of the resistance-in-series model to the experimental data. Table 3 also allows comparison between Hermia's models and the combined model. As it was explained in Section 2.2., the combined model considers the intermediate pore blocking and the cake formation mechanisms proposed by Hermia in order to predict the decline of permeate flux with time. In this case, as shown in Table 3, this combination of mechanisms resulted in a greater fitting accuracy than that obtained with the individual Hermia's models adapted to crossflow.

Table 3. Models fitting accuracy: values of R^2 and SD. Values in bold correspond to the best fitting model.

TMP[a] (bar)	CFV[b] ($m \cdot s^{-1}$)	Sample	Feed turbidity (NTU)	Complete blocking		Intermediate blocking		Cake formation		Combined model		Resistance-in-series	
				R^2	SD[c]	R^2	SD[c]	R^2	SD[c]	R^2	SD[c]	R^2	SD[c]
1	2.2	S2	314.3	0.401	0.122	0.703	0.084	0.896	0.051	0.894	0.059	**0.969**	**0.034**
	2.9	S1	367.5	0.525	0.108	0.760	0.076	0.908	0.050	0.850	0.068	**0.953**	**0.040**
2	2.2	S2	314.3	0.643	0.110	0.835	0.076	0.960	0.040	0.990	0.022	**0.989**	**0.023**
	2.9	S2	314.3	0.527	0.103	0.747	0.076	0.893	0.050	0.984	0.022	**0.985**	**0.022**
	2.9	S4	183.4	0.590	0.092	0.743	0.073	0.883	0.051	0.990	0.017	**0.988**	**0.018**
	3.7	S3	185.9	0.494	0.109	0.676	0.088	0.852	0.062	0.992	0.016	**0.986**	**0.020**
	3.7	S4	183.4	0.603	0.078	0.739	0.064	0.862	0.048	0.984	0.017	**0.980**	**0.019**
3	2.2	S3	185.9	0.713	0.140	0.889	0.094	0.986	0.038	0.995	0.023	**0.996**	**0.023**
	2.2	S1	367.5	0.186	0.187	0.376	0.168	0.665	0.122	0.984	0.034	**0.984**	**0.030**
	2.9	S3	185.9	0.670	0.120	0.836	0.089	0.961	0.048	0.996	0.017	**0.994**	**0.020**
	3.7	S3	185.9	0.626	0.105	0.783	0.082	0.919	0.053	0.994	0.015	**0.992**	**0.016**

[a]TMP: transmembrane pressure; [b]CFV: crossflow velocity; [c]SD: standard deviation.

The values of model parameters for the best fitting model (the resistance-in-series one) are shown in Table 4. As it was described in section 2.3, a high total hydraulic resistance causes great decrease in permeate flux. The total hydraulic resistance is the sum of the original membrane resistance (R_m), the adsorption and concentration polarization resistance (R_a) and the cake layer resistance (R_{cf}), according to Eq. 4. While R_m is characteristic of the membrane and remains constant during the test, R_a and R_{cf} may vary with time. The values of R_a and R_{cf} shown in the table correspond to the stationary values of the resistances. From Table 4, it can be observed that R_{cf} is greater than R_a, therefore cake formation dominated permeate flux decline at the steady state for the operating conditions considered.

Table 4. Values of model parameters for the resistance-in-series model at the different operating conditions tested.

TMP[a] (bar)	CFV[b] ($m \cdot s^{-1}$)	Sample	Feed turbidity (NTU)	Model parameters	
				R_a[c] ($\cdot 10^{13}$ m^{-1})	R_{cf}[d] ($\cdot 10^{13}$ m^{-1})
1	2.2	S2	314.3	0.661	1.730
	2.9	S1	367.5	0.669	1.557
2	2.2	S2	314.3	1.062	1.841
	2.9	S2	314.3	1.249	1.454
	2.9	S4	183.4	0.733	1.012
	3.7	S3	185.9	0.818	0.867
	3.7	S4	183.4	0.657	0.804
3	2.2	S3	185.9	1.614	2.759
	2.2	S1	367.5	2.279	2.739
	2.9	S3	185.9	1.259	1.975
	3.7	S3	185.9	1.102	1.447

[a]TMP: transmembrane pressure; [b]CFV: crossflow velocity; [c]R_a: adsorption and concentration polarization resistance; [d]R_{cf}: cake layer resistance.

Fig. 5 shows the evolution of the different resistances with time for the sample S3 at 3 bar and 3.7 $m \cdot s^{-1}$. It can be observed that at the beginning of the test predominates the adsorption and concentration polarization resistance. For all the tests performed with

different samples and at different operating conditions the trend was similar. At the beginning of the run a rapid increase of the adsorption and concentration polarization resistance (R_a) takes place. However, the increase of the cake layer resistance (R_{cf}) with time is more gradual, but it surpasses the value of R_a.

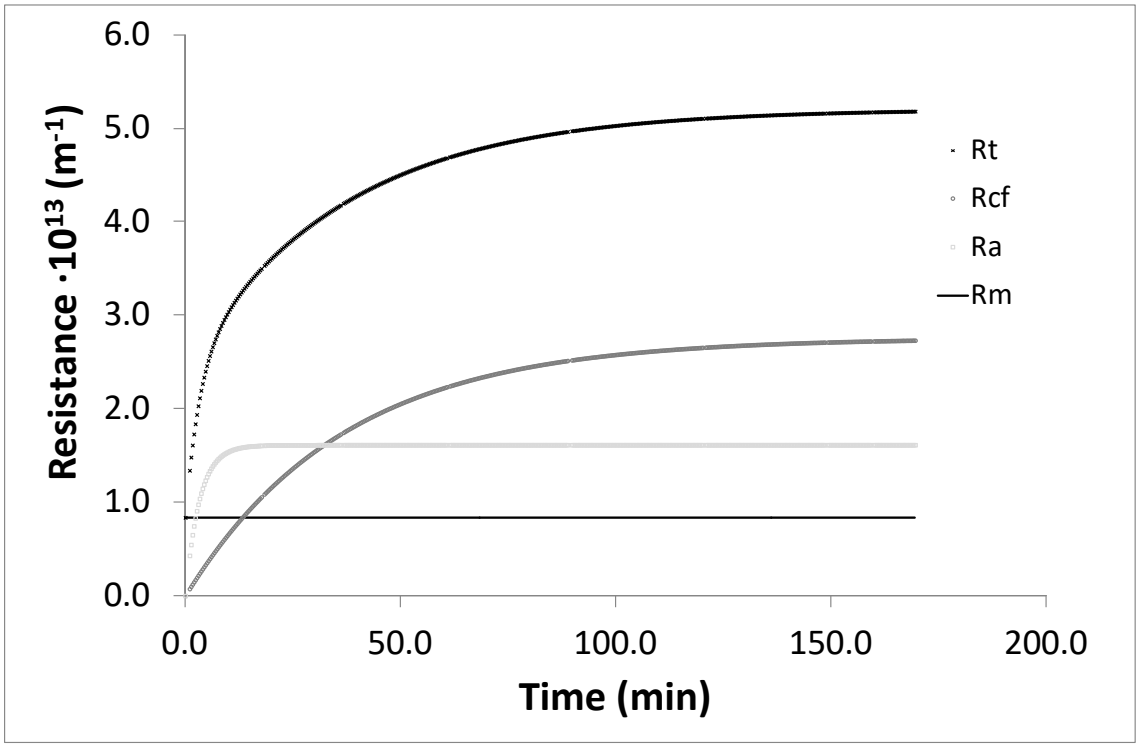

Fig. 5 Evolution of the resistances with time for sample S3 ultrafiltered at 3 bar and 2.2 $m \cdot s^{-1}$. Rt: total hydraulic resistance (m^{-1}); Rcf: cake layer resistance (m^{-1}); Ra: adsorption and concentration polarization resistance (m^{-1}); Rm: membrane resistance (m^{-1}).

As it was abovementioned, the initial permeate flux decline with time is due to the pore blocking phenomena. As it can be observed in Figs. 1-3, the higher the transmembrane pressure was, the more rapid the permeate flux decline was during the first minutes of the UF process. Several authors (Ho and Zydney, 2000; de la Casa et al. 2008; Mondal and De, 2010) reported that the evolution of permeate flux with time can be divided in two stages: the first one is caused by pore blocking and adsorption phenomena during the first minutes of operation and results in a rapid flux decline; while the second step is

due to the formation and growth of a cake layer on the membrane surface, which leads to a slow flux decline until a steady-state value is achieved. This pattern is related to the values of R_a and R_{cf}. The parameter R_a is related to the pore blocking and absorption mechanism and the parameter R_{cf} is related to the cake formation. It is expected that, as transmembrane pressure increases, the values of R_a also increase, due to the more severe decrease in permeate flux observed in Fig. 3 compared to Fig. 1. This trend is clearly observed in Table 4 for all the crossflow velocities tested when transmembrane pressure increased from 1 to 3 bar independently of the feed sample. Regarding the effect of crossflow velocity on R_a, it can be observed that this parameter decreased as crossflow velocity increased. For example, the values of R_a for sample S3 (turbidity of 185.9 NTU) at a transmembrane pressure of 3 bar decreased from $16.140 \cdot 10^{12}$ to $12.590 \cdot 10^{12}$ and then to $11.020 \cdot 10^{12}$ when crossflow velocity increased from 2.2 to 2.9 and then to 3.7 $m \cdot s^{-1}$, respectively. A few exceptions to this trend can be explained as a result of the different turbidity of the samples. For the same operating conditions R_a increased when feed turbidity increased, as it can be observed for samples S2 and S4 at 2 bar and 2.9 $m \cdot s^{-1}$ and for samples S1 and S3 at 3 bar and 3.7 $m \cdot s^{-1}$. On the other hand, regarding the cake formation parameter, as crossflow velocity increased R_{cf} decreased, for all the transmembrane pressures tested. This is explained by the reduction of the fouling layer formed on the membrane surface during the UF process because of the increase in the shear stress. Also, for a fixed crossflow velocity, R_{cf} increased when transmembrane pressures increased. However, R_{cf} for sample S1 ultrafiltered at 1 bar and 2.9 $m \cdot s^{-1}$ was greater than that for samples S2 and S4 at 2 bar and 2.9 $m \cdot s^{-1}$. This is due to the effect of turbidity, as sample S1 was the one with higher turbidity. Also, for the same operating conditions R_{cf} increased when turbidity increased, as it can be observed for

sample S2 and sample S4 at 2 bar and 2.9 $m \cdot s^{-1}$. For high TMP and low CFV R_{cf} had similar values even for samples with very different turbidity.

4.2. Validation of resistance-in-series model

In order to validate the resistance-in-series model, the combined resistance model proposed by Mondal and De was used, as it was explained in Section 2.4 (Mondal and De, 2010). For this purpose, the resistance of the cake layer previously determined by the resistance-in-series model was taken into account. Table 5 shows the fitting accuracy results for the combined resistance model proposed by Mondal and De.

Table 5. Fitting accuracy for the model developed by Mondal and De (Mondal and De, 2010) when the resistance-in-series parameters were considered: values of R^2 and SD.

TMP[a] (bar)	CFV[b] ($m \cdot s^{-1}$)	Sample	Feed turbidity (NTU)	Mondal & De vs experimental data		Mondal & De vs resistance-in-series	
				R^2	SD[c]	R^2	SD[c]
1	2.2	S2	314.3	0.966	0.034	0.997	0.006
	2.9	S1	367.5	0.912	0.050	0.957	0.033
2	2.2	S2	314.3	0.976	0.029	0.991	0.015
	2.9	S2	314.3	0.978	0.024	0.993	0.010
	2.9	S4	183.4	0.976	0.022	0.993	0.009
	3.7	S3	185.9	0.965	0.031	0.985	0.020
	3.7	S4	183.4	0.963	0.023	0.992	0.010
3	2.2	S3	185.9	0.979	0.040	0.987	0.030
	2.2	S1	367.5	0.974	0.036	0.993	0.016
	2.9	S3	185.9	0.981	0.026	0.993	0.013
	3.7	S3	185.9	0.975	0.025	0.989	0.015

[a]TMP: transmembrane pressure; [b]CFV: crossflow velocity; [c]SD: standard deviation.

Permeate flux predicted by the model proposed by Mondal and De was compared to the the experimental data and also to permeate flux predicted by the resistance-in-series model. The fitting accuracy results were expressed in terms of the regression coefficient (R^2) and standard deviation (SD). As it can be observed, when model predictions are

compared to the experimental data the accuracy was higher than 95% for all the runs except one (sample S1 ultrafiltered at 1 bar and 2.9 $m \cdot s^{-1}$). The standard deviation for the rest of the tests was between 0.040 – 0.022. The accuracy of the prediction considering the permeate flux data obtained with the resistance in series method was higher than 95% in all test with a standard deviation between 0.033 – 0.006. This indicates that both models predicted similar values of permeate flux and also the value R_{cf} is equivalent in both ones.

Fig. 6 compares permeate flux decline with time predicted by the resistance-in-series model to that predicted by the combined resistance method proposed by Mondal and De and to the experimental data for sample S3 ultrafiltered at 3 bar and 2.2 $m \cdot s^{-1}$.

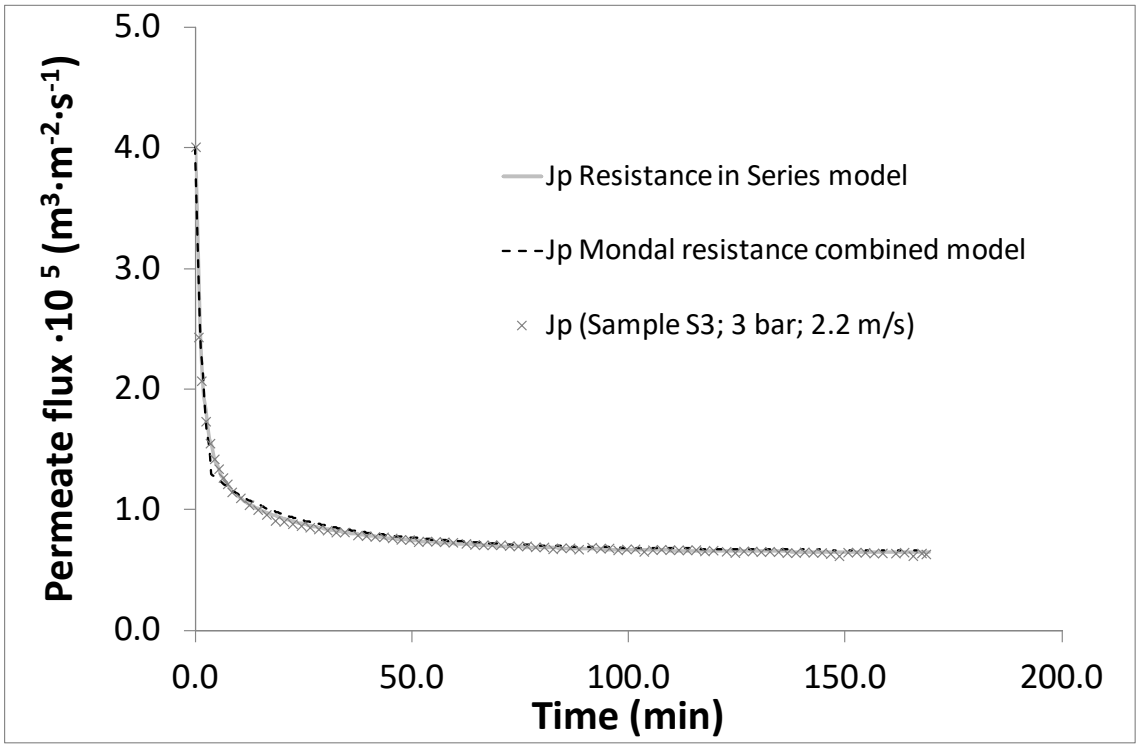

Fig. 6 Comparison between the experimental permeate flux observed for sample S3 at 3 bar and 2.2 $m \cdot s^{-1}$, the permeate flux predicted by the resistance-in-series model and the permeate flux predicted by the combined resistance model proposed by Mondal and De (Mondal and De, 2010).

The figure shows very similar predictions for both models with a sharp initial reduction of permeate flux. Nevertheless, permeate flux predicted by the resistance-in-series model is closer to the experimental observations.

5. Conclusions

Three different mathematical models (Hermia's models adapted to crossflow UF, a combined model and a resistance-in-series one) were fitted to the experimental data of permeate flux decline with time obtained with a 5 kDa PES UF membrane when different samples of table olive production wastewaters were used as feed solutions. Among all the models taken into account, the resistance-in-series model that considered pore blocking and absorption, and cake formation fouling mechanisms was the most accurate in terms of high R^2 and low SD for all the transmembrane pressures, crossflow velocities and different feed solutions tested. Therefore, pore blocking and absorption, and cake formation were the predominant fouling mechanisms that explained the decline of permeate flux with time.

The influence of transmembrane pressure and crossflow velocity on the values of the resistance-in-series model parameters was determined. As transmembrane pressure increased the adsorption and concentration polarization resistance (R_a) and the cake layer resistance (R_{cf}) increased. As crossflow velocity increased, R_a slightly decreased or keeps constant and R_{cf} decreased. As the turbidity of the feed sample increased R_a and R_{cf} increased. In the steady state R_{cf} was the predominant fouling mechanism for the operating conditions considered. The predominant fouling mechanism in the first minutes of the UF tests was R_a.

The combined resistance model proposed by Mondal and De, 2010 was evaluated as well and the predictions were similar to that of the resistance-in-series model. It was observed that the cake layer resistance was equivalent for both models.

Acknowledgements

The authors of this work wish to gratefully acknowledge the financial support of CDTI (Centre for Industrial Technological Development) depending on the Spanish Ministry of Science and Innovation.

Nomenclature

List of symbols

b	Fouling rate due to adsorption (s^{-1})
K	Hermia's model constant (units depending on n)
K_c	Complete blocking model constant (s^{-1})
K_{cf}	Cake layer formation model constant ($s \cdot m^{-2}$)
J	Permeate flux ($m^3 \cdot m^{-2} \cdot s^{-1}$)
J_{model}	Permeate flux predicted by each model ($m^3 \cdot m^{-2} \cdot s^{-1}$)
J_{ss}	Steady-state permeate flux ($m^3 \cdot m^{-2} \cdot s^{-1}$)
n	Hermia's model parameter (dimensionless)
P	Transmembrane pressure (bar)
R	Total hydraulic resistance (m^{-1})

R_a Resistance due to adsorption on membrane surface and inside its pores and concentration polarization (m^{-1})

R'_a Steady-state adsorption and concentration polarization resistance (m^{-1})

R_{cf} Cake layer resistance (m^{-1})

R_m New membrane resistance (m^{-1})

t Filtration time (s)

Greek letters

α Fraction of membrane pores completely blocked (dimensionless)

μ Feed solution viscosity ($kg \cdot m^{-1} \cdot s^{-1}$)

Abbreviations

CFV Crossflow velocity ($m \cdot s^{-1}$)

COD Chemical oxygen demand

MWCO Molecular weight cut off

NF Nanofiltration

NTU Nephelometric Turbidity Unit

OMW Olive mill wastewater

PES Polyethersulfone

SD Standard deviation

TMP Transmembrane pressure (bar)

TOPP Table olive packing plant

TSS Total suspended solids

UF Ultrafiltration

References

Alburquerque, J.A., Gonzálvez, J., García, D., Cegarra, J.: Agrochemical characterisation of “alperujo”, a solid by-product of the two-phase centrifugation method for olive oil extraction. Bioresour. Technol. 91 (2004) 195–200, doi:10.1016/S0960-8524(03)00177-9

Astaree, R.S., Mohammadi, T., Kasiri, N.: Analysis of BSA, dextran and humic acid fouling during microfiltration, experimental and modeling. Food Bioprod. Process. 94 (2015) 331-341, doi:10.1016/j.fbp.2014.04.003

Astudillo-Castro, C.: Limiting flux and critical transmembrane pressure determination using an exponential model: the effect of concentration factor, temperature, and cross-flow velocity during casein micelle concentration by microfiltration. Ind. Eng. Chem. Res. 54 (2015) 414–425, doi: 10.1021/ie5033292

Barredo-Damas, S., Alcaina-Miranda, M.I., Iborra-Clar, M.I., Mendoza-Roca, J.A.: Application of tubular ceramic ultrafiltration membranes for the treatment of integrated textile wastewaters. Chem. Eng. J. 192 (2012) 211–218, doi:10.1016/j.cej.2012.03.079

Benitez, J. F., Acero, J.L., Leal, A. I.: Purification of storage brines from the preservation of table olives. J. Hazard. Mater. 96 (2003) 155–169. doi:10.1016/S0304-3894(02)00183-8

Bódalo, A., Gómez, J.L., Gómez, M., León, G., Hidalgo, A.M., Ruíz, M.A.: Phenol removal from water by hybrid processes: study of the membrane process step. Desalination 223 (2008) 323–329, doi:10.1016/j.desal.2007.01.219

Bolton, G., LaCasse, D., Kuriyel, R.: Combined models of membrane fouling: Development and application to microfiltration and ultrafiltration of biological fluids. J. Membr. Sci. 277 (2006) 75-84, doi:10.1016/j.memsci.2004.12.053

Carrère, H., Blaszkow, F., Roux de Balmann, H.: Modelling the clarification of lactic acid fermentation broths by cross-flow microfiltration. J. Membr. Sci. 186 (2001) 219-230, doi:10.1016/S0376-7388(00)00677-3

Carrère, H., Blaszkow, F., Roux de Balmann, H.: Modelling the microfiltration of lactic acid fermentation broths and comparison of operating modes. Desalination 145 (2002) 201–206 doi:10.1016/S0011-9164(02)00409-5

Chen, H., Kim, A.S.: Prediction of permeate flux decline in crossflow membrane filtration of colloidal suspension: a radial basis function neural network approach. Desalination 192 (2006) 415–428, doi:10.1016/j.desal.2005.07.045

Cheryan, M., Alvarez, J.R.: Food and beverage industry applications, Membrane Separation Technology, Principles and Applications, Ed. R.D. Noble, University of Colorado, Boulder, CO, USA and S.A. Stern, Syracuse University, Syracuse, NY, USA (1995) 341, ISBN: 978-0-444-81633-7

Choi, S-W., Yoon, J-Y., Haam, S., Jung, J-K., Kim, J-H., Kim, W-S.: Modeling of the permeate flux during microfiltration of BSA-adsorbed microspheres in a stirred cell. J. Colloid Interface Sci. 228 (2000) 270-278, doi:10.1006/jcis.2000.6940

Corbatón-Báguena, M.J., Vincent-Vela, M.C., Álvarez-Blanco, S., Lora-García, J.: Analysis of two ultrafiltration fouling models and estimation of model parameters as a function of operational conditions. Transp. Porous Media 99 (2013) 391–411, doi: 10.1007/s11242-013-0192-4

Corbatón-Báguena, M.J., Álvarez-Blanco, S., Vincent-Vela, M.C.: Fouling mechanisms of ultrafiltration membranes fouled with whey model solutions. Desalination 360 (2015a) 87-96, doi:10.1016/j.desal.2015.01.019

Corbatón-Báguena, M.J., Gugliuzza, A., Cassano, A. Mazzei, R., Giorno, L.: Destabilization and removal of immobilized enzymes adsorbed onto polyethersulfone ultrafiltration membranes by salt solutions. J. Membr. Sci. 486 (2015b) 207-214, doi:10.1016/j.memsci.2015.03.061

de Barros, S.T.D., Andrade, C.M.G., Mendes, E.S., Peres, L.: Study of fouling mechanism in pineapple juice clarification by ultrafiltration. J. Membr. Sci. 215 (2003) 213-224 doi:10.1016/S0376-7388(02)00615-4

de la Casa, E.J., Guadix, A., Ibáñez, R., Camacho, F., Guadix, E.M.: A combined fouling model to describe the influence of the electrostatic environment on the cross-flow microfiltration of BSA. J. Membr. Sci. 318 (2008) 247-254, doi:10.1016/j.memsci.2008.02.047

El-Abbassi, A., Kiai, H., Raiti, J., Hafidi A.: Application of ultrafiltration for olive processing wastewaters treatment. J. Cleaner Prod. 65 (2014) 432–438, doi:10.1016/j.jclepro.2013.08.016

Field, R.W., Wu, D., Howell, J.A., Gupta, B.B.: Critical flux concept for microfiltration fouling. J. Membr. Sci 100 (1995) 259–272, doi:10.1016/0376-7388(94)00265-Z

Galanakis, C.M., Tornberg, E., Gekas, V.: Clarification of high-added value products from olive mill wastewater. J. Food Eng. 99 (2010) 190–197, doi:10.1016/j.jfoodeng.2010.02.018

Garrido Fernández, A., Fernández Díez, M.J., Adams, R.M.: Table olives. Production and processing. Chapman & Hall, UK London (1997), ISBN 978-0412718106

Hermia J.: Constant pressure blocking filtration laws – application to powerlaw non-newtonian fluids. Inst. Chem. Eng. 60 (1982) 183-187.

Ho, C-C., Zydney, A.L.: A combined pore blockage and cake filtration model for protein fouling during microfiltration. J. Colloid Interface Sci. 232 (2000) 389-399, doi:10.1006/jcis.2000.7231

International Olive Oil Council. Compiled data taken from the total produced worldwide of total table olives by country, (2014)

Karasu, K., Yoshikawa, S., Ookawara, S., Ogawa, K., Kentish, S.E., Steves, G.W.: A combined model for the prediction of the permeation flux during the cross-flow ultrafiltration of a whey suspension. J. Membr. Sci. 361 (2010) 71-77, doi:10.1016/j.memsci.2010.06.008

Lin, C.-J., Rao, P., Shirazi, S.: Effect of operating parameters on permeate flux decline caused by cake formation - a model study. Desalination 171 (2004) 95-105, doi:10.1016/j.desal.2004.03.023

Lin, S.-H., Hung, C.-L., Juang, R.-S.: Applicability of the exponential time dependence of flux decline during dead-end ultrafiltration of binary protein solutions. Chem. Eng. J. 145 (2008) 211-217, doi:10.1016/j.cej.2008.04.003

Liu, H., Tang, Z., Cui, C., Sun, C., Zhu, H., Li, B., Guo, L.: Fouling mechanisms of the extract of traditional Chinese medicine in ultrafiltration. Desalination 354 (2014) 87-96, doi:10.1016/j.desal.2014.09.016

Mah, S-K., Chuah, C-K., Cathie Lee, W.P., Cahi, S-P.: Ultrafiltration of palm oil-oleic acid-glycerin solutions: Fouling mechanism identification, fouling mechanism analysis and membrane characterizations. Sep. Purif. Technol. 98 (2012) 419-431, doi:10.1016/j.seppur.2012.07.020

Miller, D.J., Kasemset, S., Paul, D.R., Freeman, B.D.: Comparison of membrane fouling at constant flux and constant transmembrane pressure conditions. J. Membr. Sci. 454 (2014) 505–515, doi:10.1016/j.memsci.2013.12.027

Mondal, S., Cassano, A., Tasselli, F., De, S.: A generalized model for clarification of fruit juice during ultrafiltration under total recycle and batch mode. J. Membr. Sci. 366 (2011) 295–303, doi:10.1016/j.memsci.2010.10.015

Mondal, S., De, S.: A fouling model for steady state crossflow membrane filtration considering sequential intermediate pore blocking and cake formation. Sep. Purif. Technol. 75 (2010) 222-228, doi:10.1016/j.seppur.2010.07.016

Mondal, S., De, S.: Generalized criteria for identification of fouling mechanism under steady state membrane filtration. J. Membr. Sci. 344 (2009) 6-13, doi:10.1016/j.memsci.2009.08.015

Muthukumaran, S., Kentish, S.E., Ashokkumar, M., Stevens, G.W.: Mechanisms for the ultrasonic enhancement of dairy whey ultrafiltration. J. Membr. Sci. 258 (2005) 106-114, doi:10.1016/j.memsci.2005.03.001

Paraskeva, C.A., Papadakis, V.G., Tsarouchi, E., Kanellopoulou, D.G., Koutsoukos, P.G.: Membrane processing for olive mill wastewater fractionation. Desalination 213 (2007) 218-229, doi:10.1016/j.desal.2006.04.087

Paredes, C., Cegarra, J., Roig, A., Sánchez-Monedero, M.A., Bernal, M.P.: Characterization of olive mill wastewater (alpechin) and its sludge for agricultural purposes. Bioresour. Technol. 67 (1999) 111–115, doi:10.1016/S0960-8524(98)00106-0

Peng, H., Tremblay, A.Y.: Membrane regeneration and filtration modeling in treating oily wastewaters. J. Membr. Sci. 324 (2008) 59-66, doi:10.1016/j.memsci.2008.06.062

Rezaei, H., Ashtiani, F.Z., Fouladitajar, A.: Effects of operating parameters on fouling mechanism and membrane flux in cross-flow microfiltration of whey. Desalination 274 (2011) 262-271, doi:10.1016/j.desal.2011.02.015

Ruby Figueroa, R.A., Cassano, A., Drioli, E.: Ultrafiltration of orange press liquor: optimization for permeate flux and fouling index by response surface methodology. Sep. Purif. Technol. 80 (2011) 1–10, doi:10.1016/j.seppur.2011.03.030

Tien, C., Ramarao, B.V., Yasarla, R.: A blocking model of membrane filtration. Chem. Eng. Sci. 111 (2014) 421-431, doi:10.1016/j.ces.2014.01.022

Turano, E., Curcio, S., De Paola, M.G., Calabrò, V., Iorio, G.: An integrated centrifugation-ultrafiltration system in the treatment of olive mil wastewater. J. Membr. Sci. 209 (2002) 519-531, doi:10.1016/S0376-7388(02)00369-1

Vincent Vela, M.C., Álvarez Blanco, S., Lora García, J., Bergatiños Rodríguez, E.: Analysis of membrane pore blocking models adapted to crossflow ultrafiltration in the ultrafiltration of PEG. Chem. Eng. J. 149 (2009) 232-241, doi:10.1016/j.cej.2008.10.027

Vincent-Vela, M.C., Cuartas-Uribe, B., Álvarez-Blanco S., Lora-García J., Bergantiños-Rodríguez, E.: Analysis of ultrafiltration processes with dilatant macromolecular solutions by means of dimensionless numbers and hydrodynamic parameters. Sep. Purif. Technol. 75 (2010) 332–339, doi:10.1016/j.seppur.2010.09.001

Wang, L., Song, L.: Flux decline in crossflow microfiltration and ultrafiltration: experimental verification of fouling dynamics. J. Membr. Sci. 160 (1999) 41–50, doi:10.1016/S0376-7388(99)00075-7

Yee, K.W.K., Wiley, D.E., Bao, J.: A unified model of the time dependence of flux decline for the long-term ultrafiltration of whey. J. Membr. Sci. 332 (2009) 69-80, doi:10.1016/j.memsci.2009.01.041